

Thermodynamic anomalies in a lattice model of water

M. Pretti and C. Buzano

*Istituto Nazionale per la Fisica della Materia (INFM) and Dipartimento di Fisica,
Politecnico di Torino, Corso Duca degli Abruzzi 24, I-10129 Torino, Italy*

(Dated: December 29, 2021)

We investigate a lattice-fluid model of water, defined on a three-dimensional body centered cubic lattice. Model molecules possess a tetrahedral symmetry, with four equivalent bonding arms, aiming to mimic the formation of hydrogen bonds. The model is similar to the one proposed by Roberts and Debenedetti [J. Chem. Phys. **105**, 658 (1996)], simplified in that no distinction between bond “donors” and “acceptors” is imposed. Bond formation depends both on orientation and local density. In the ground state, we show that two different ordered (ice) phases are allowed. At finite temperature, we analyze homogeneous phases only, working out phase diagram, response functions, the temperature of maximum density locus, and the Kauzmann line. We make use of a generalized first order approximation on a tetrahedral cluster. In the liquid phase, the model exhibits several anomalous properties observed in real water. In the low temperature region (supercooled liquid), there are evidences of a second critical point and, for some range of parameter values, this scenario is compatible with the existence of a reentrant spinodal.

PACS numbers: 61.20.-p, 64.60.Cn, 64.60.My, 65.20.+w

I. INTRODUCTION

It is a well known fact that several thermodynamic properties of water exhibit some anomalous behavior^{1,2,3}. First of all, the heat capacity is unusually large and, at ordinary pressures, the solid phase (ice) is less dense than the liquid. Moreover, the liquid phase displays a temperature of maximum density at constant pressure, while both isothermal compressibility and isobaric heat capacity have a minimum as a function of temperature. Generally speaking, the anomalous properties can be explained by the ability of water molecules to form hydrogen bonds, and by the peculiar features of such kind of bonds^{4,5}. The same physics is thought to underly the unusual properties of water as a solvent for apolar compounds^{6,7}, that is of the hydrophobic effect, whose importance in biophysics has been recognized in the latest years⁸. Nevertheless, a comprehensive theory which explains all of these phenomena has not been developed yet.

“Realistic” simulations of water^{9,10,11,12}, based on more and more refined (but still phenomenological) interaction potentials, have reached quite a high level of accuracy in describing water thermodynamics. Nevertheless, they are intrinsically limited by the large computational effort required, which becomes still larger when it is necessary to determine multiple derivatives of the free energy, such as response functions. Moreover, due to the high level of microscopic detail, both of geometry and of interactions, often they do not make it easy to discriminate what is essential to explain macroscopic properties. On the contrary, simplified models need simpler numerical calculations and, even if their quantitative accuracy is often poor, it is generally easier to trace connections between microscopic interactions and macroscopic properties^{13,14,15,16,17,18,19,20,21,22,23,24}. A simplified mechanism, proposed to account for the significant anomalies of water is the following one (see for instance Refs. 5,25).

The formation of a hydrogen bond requires that two molecules assume certain relative orientations, staying at a distance larger than the one needed to minimize Van der Waals energy. This fact gives rise to a competition between the two kinds of interaction. Optimizing Van der Waals interaction allows *higher density* and *higher orientational entropy*, but yields a *weaker binding energy*, whereas, optimizing hydrogen bonding requires a *lower density* and a *lower orientational entropy*, but gives rise to a *stronger binding energy*. Therefore, at low enough temperature, local density and entropy fluctuations may become positively correlated, thus rationalizing a change of sign of the thermal expansion coefficient, that is a density maximum. Such a simple mechanism has been implemented by different models, both on-^{22,23,26,27,28} and off-lattice²⁴, in 3^{22,23} as well as 2 dimensions^{24,26,27,28}.

One of them is the 3-dimensional model proposed by Roberts and Debenedetti (RD)^{23,29}, defined on the body centered cubic lattice. Model molecules possess four bonding arms (two donors and two acceptors) arranged in a tetrahedral symmetry. Working on a lattice, one has to resort to a trick to describe hydrogen bond weakening, when the two participating molecules are too close to each other. Such a trick is defined as follows. The energy of any formed bond is increased of some fraction (weakened bond) by the presence of a third molecule on a site close to the bond. Let us notice that the model has the same bonding properties as the early model proposed by Bell¹⁵, but the weakening criterion is different. The RD model is quite appealing in that it has been shown to predict some of real water thermodynamic anomalies, such as the temperature of maximum density, also showing evidence of a liquid-liquid phase separation in the supercooled region, and of a second critical point. In view of investigations on mixtures of water with other chemical species, as is the case, for instance, in most biological processes, it would be desirable to obtain an even simpler

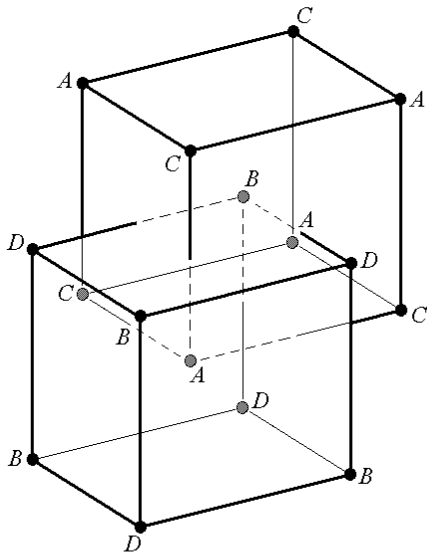


FIG. 1: Two conventional cells of the body centered cubic lattice: A, B, C, D denote 4 interpenetrating face centered cubic sublattices.

model, capable of capturing the same essential features. As it has been pointed out by other authors^{24,30}, the distinction between donors and acceptors is likely to be not so crucial to describe the physics of hydrogen bonding. Therefore, a simplified version of the RD model, without a distinction between hydrogen bond donors and acceptors, might be a good compromise between simplicity and accuracy.

In this paper we investigate such a model, with a twofold purpose. As mentioned above, we are meant to explore the possibility of obtaining a simpler model with the same underlying physical mechanism, and with qualitatively the same macroscopic properties. In addition, we are interested in providing a more detailed analysis of the effect of the weakening parameter, which turns out to be extremely relevant to determine the phase diagram, mainly in the supercooled liquid region. The paper is organized as follows. In Sec. II we define the model and analyze its ground state. In Sec. III we introduce the first order approximation in a cluster variational formulation (cluster-site approximation), which we employ for the analysis. Sec. IV describes the results and Sec. V is devoted to some concluding remarks. An Appendix reports the calculation of density response functions and spinodals for the liquid phase.

II. THE MODEL AND THE GROUND STATE

Let us first introduce the model. Molecules are placed on the sites of a body centered cubic lattice, whose structure is sketched in Fig. 1. A site may be empty or occupied by a water molecule. An attractive potential energy $-\epsilon < 0$ is assigned to any pair of nearest neighbor (NN)

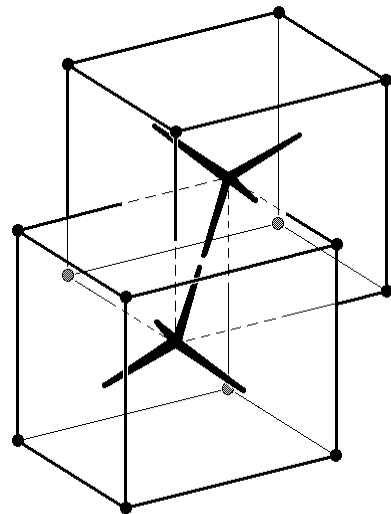


FIG. 2: Two model molecules forming a H bond. The lower molecule is in the $i = 1$ configuration, the upper one is in the $i = 2$ configuration.

occupied sites. This is the ordinary Van der Waals contribution. In the RD model, water molecules possess four arms that can form hydrogen (H) bonds (two donors and two acceptors), arranged in a tetrahedral symmetry, so that they can point towards 4 out of 8 NNs of a given site. We assume for simplicity that donors and acceptors are undistinguishable, that is a H bond is formed whenever two NN molecules have a bonding arm pointing to each other, yielding an energy $-\eta < 0$. Without such a distinction, it turns out that a water molecule has only 2 different configurations in which it can form H bonds (see Fig. 2). We assume that w more configurations are allowed, in which the molecule cannot form bonds. The w parameter is related to the bond-breaking entropy. Moreover, to account for the fact that H bonds are most favorably formed when water molecules are located at a certain distance, larger than the optimal Van der Waals distance, the RD model assigns an energy increase $\eta c/6$, with $c \in [0, 1]$, for each of the 6 sites closest to the bond occupied by a water molecule (i.e., 3 out of 6 second neighbors of each participating molecule). A bond surrounded by all 6 water molecules is “fully weakened” and contributes an energy $-\eta(1 - c)$.

The hamiltonian of the system can be written as a sum over irregular tetrahedra, whose vertices lie on 4 different face-centered cubic sublattices, shown in Fig. 1. One of such tetrahedra is shown in Fig. 3(a). We have

$$\mathcal{H} = \frac{1}{6} \sum_{\langle \alpha, \beta, \gamma, \delta \rangle} \mathcal{H}_{i_\alpha i_\beta i_\gamma i_\delta}, \quad (1)$$

where \mathcal{H}_{ijkl} is a contribution which will be referred to as tetrahedron hamiltonian, and the subscripts $i_\alpha, i_\beta, i_\gamma, i_\delta$ label site configurations for the 4 vertices $\alpha, \beta, \gamma, \delta$, respectively. Possible configurations are: Empty site ($i =$

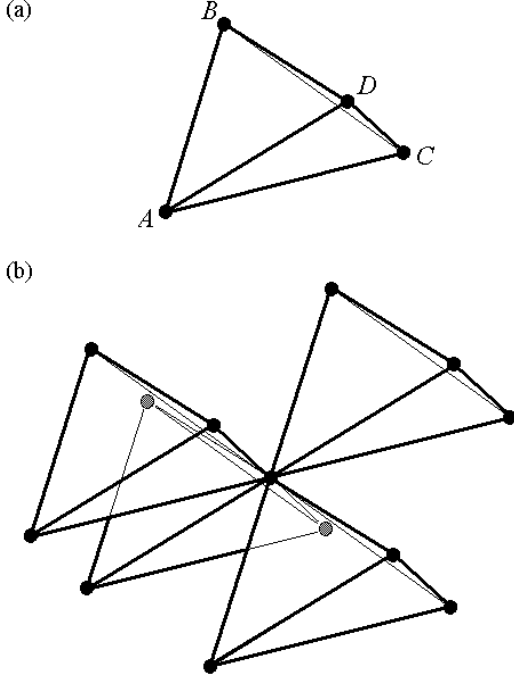


FIG. 3: (a) Basic cluster (irregular tetrahedron): A, B, C, D denote sites in the 4 corresponding sublattices. AB, BC, CD , and DA are NN pairs; AC and BD are second neighbor pairs. (b) Husimi tree structure corresponding to the generalized first order approximation on the tetrahedron.

0), site occupied by a molecule in one of 2 bonding orientations ($i = 1, 2$; see Fig. 2) or in one of w non-bonding configurations ($i = 3$). Assuming that (i, j) , (j, k) , (k, l) , and (l, i) refer to NN pair configurations, the tetrahedron hamiltonian reads

$$\begin{aligned} \mathcal{H}_{ijkl} = & -\epsilon(n_i n_j + n_j n_k + n_k n_l + n_l n_i) \\ & -\eta \left[h_{ij} \left(1 - c \frac{n_k + n_l}{2} \right) + h_{jk} \left(1 - c \frac{n_l + n_i}{2} \right) \right. \\ & \left. + h_{kl} \left(1 - c \frac{n_i + n_j}{2} \right) + h_{li} \left(1 - c \frac{n_j + n_k}{2} \right) \right], \end{aligned} \quad (2)$$

where n_i is an occupation variable, defined as $n_i = 0$ for $i = 0$ (empty site) and $n_i = 1$ otherwise (occupied site), while $h_{ij} = 1$ if the pair configuration (i, j) forms a H bond, and $h_{ij} = 0$ otherwise. Let us also assume that i, j, k, l (in this order) denote configurations of sites placed on, say, A, B, C, D sublattices respectively. If A, B, C, D are defined as in Fig. 1, we can define $h_{ij} = 1$ if $i = 1$ and $j = 2$, and $h_{ij} = 0$ otherwise. With the above assumptions, the tetrahedron hamiltonian is independent of the orientation, that is of the arrangement of A, B, C, D on its vertices. This is a nice effect of removing the donor-acceptor distinction, which considerably simplifies the whole analysis. Let us notice that both Van der Waals ($-\epsilon n_i n_j$) and H bond energies ($-\eta h_{ij}$), which are 2-body terms, are split among 6 tetrahedra, whence the $1/6$ prefactor in Eq. (1). On the contrary, the 3-body

weakening terms ($\eta c h_{ij} n_k / 6$) are split between 2 tetrahedra, thus the $1/6$ factor is absorbed in the prefactor, while a $1/2$ factor is left in the tetrahedron hamiltonian. Let us denote the tetrahedron configuration probability by p_{ijkl} , with the same convention about the subscript order, and assume that the probability distribution is equal for every tetrahedron. Taking into account that there are 6 tetrahedra per site, we can write the following expression for the internal energy per site of an infinite lattice

$$u = \sum_{i=0}^3 w_i \sum_{j=0}^3 w_j \sum_{k=0}^3 w_k \sum_{l=0}^3 w_l p_{ijkl} \mathcal{H}_{ijkl}. \quad (3)$$

The multiplicity for the tetrahedron configuration (i, j, k, l) is given by $w_i w_j w_k w_l$, where $w_i = w$ for $i = 3$ (non-bonding configuration) and $w_i = 1$ otherwise (bonding configuration or vacancy).

Let us now have a look at the ground state of the model. In order to do so, let us investigate the zero temperature grand-canonical free energy $\omega^\circ = u - \mu \rho$ (μ being the chemical potential and ρ the density, i.e., the average site occupation probability), which can be formally written in the same way as the internal energy u of Eq. (3), replacing the tetrahedron hamiltonian \mathcal{H}_{ijkl} by

$$\tilde{\mathcal{H}}_{ijkl} = \mathcal{H}_{ijkl} - \mu \frac{n_i + n_j + n_k + n_l}{4}. \quad (4)$$

First of all, we have an infinitely dilute “gas” phase (G) with zero density and zero free energy. Secondly, we can conceive an ordered “open” ice phase (O) with two fully occupied sublattices, say A and B , while the other sublattices, C and D , are empty ($\rho = 1/2$). In this configuration all molecules are fully bonded, i.e., there are 2 bonds per molecule, and no bond is weakened, so that the free energy turns out to be

$$\omega_G^\circ = -\epsilon - \eta - \mu/2. \quad (5)$$

Another possibility is the “closed” ice phase (C), in which all sites are occupied ($\rho = 1$), the maximum number of H bonds is formed (for instance, all AB and CD pairs are bonded), but all bonds are fully weakened. The resulting free energy is

$$\omega_C^\circ = -4\epsilon - 2\eta(1 - c) - \mu. \quad (6)$$

It is easy to show that the G phase is thermodynamically favored ($0 < \omega_G^\circ$ and $0 < \omega_C^\circ$) for $\mu < \mu_{GO}$, where

$$\mu_{GO} = -2\epsilon - 2\eta, \quad (7)$$

the O phase is favored ($\omega_O^\circ < 0$ and $\omega_C^\circ < \omega_O^\circ$) for $\mu_{GO} < \mu < \mu_{OC}$, where

$$\mu_{OC} = -6\epsilon - 2\eta(1 - 2c), \quad (8)$$

and the C phase is favored ($\omega_C^\circ < 0$ and $\omega_C^\circ < \omega_O^\circ$) for $\mu > \mu_{OC}$. The O phase has actually a stability region, i.e., $\mu_{GO} < \mu_{OC}$, provided

$$c > \epsilon/\eta. \quad (9)$$

We shall always work in the latter regime, which allows to reproduce two different forms of ice. Even if in the following we shall not deal with ordered phases at finite temperature, the latter choice should be the most reasonable one, in order to describe real water properties. We have considered also the possibility of different structured phases, respectively with 1 or 3 occupied sublattices, but they never turn out to be stable, in the physical range of parameter values.

III. FIRST ORDER APPROXIMATION

We perform the finite temperature analysis by means of a generalized first order approximation on a tetrahedron cluster. Let us introduce the approximation in the framework of the cluster variation method, an improved mean-field theory which in principle can take into account correlations at arbitrarily large, though finite, distances. In Kikuchi's original work³¹, an approximate entropy expression was obtained by heuristic arguments, while, in more recent and rigorous formulations³², the approximation is shown to be equivalent to a truncation of a cluster cumulant expansion of the entropy. The approximation is expected to work, because of a rapid decreasing of the cumulant magnitude, upon increasing the cluster size, namely when the latter becomes larger than the correlation length of the system³³. A particular approximation is defined by the largest clusters left in the truncated expansion, usually denoted as basic clusters. One obtains a free energy functional in the cluster probability distributions, to be minimized, according to the variational principle of statistical mechanics.

For our model we choose a number of irregular tetrahedra as basic clusters, namely 4 out of 24 tetrahedra sharing a given site, as sketched in Fig. 3. This choice actually turns out to coincide with the (generalized) first order approximation (on the tetrahedron cluster), which is also equivalent to an exact calculation on a Husimi lattice³⁴, whose (tetrahedral) building blocks are just arranged as in Fig. 3(b). Such an approximation has not only the advantage of high simplicity, due to the fact that the only clusters retained in the expansion are basic clusters and single sites (it is sometimes referred to as cluster-site approximation³⁵), but also of a relative accuracy, which has been recognized for different models, even with orientation dependent interactions²⁸. Let us notice that the internal energy is treated exactly, because the range of interactions does not exceed the basic cluster size. The grand canonical free energy per site $\omega = u - Ts - \mu\rho$ (T being the temperature and s the entropy per site) can be written as

$$\begin{aligned} \frac{\omega}{T} = & \sum_{i=0}^3 w_i \sum_{j=0}^3 w_j \sum_{k=0}^3 w_k \sum_{l=0}^3 w_l p_{ijkl} \left(\frac{\tilde{\mathcal{H}}_{ijkl}}{T} + \ln p_{ijkl} \right) \\ & - 3 \sum_{i=0}^3 w_i p_i \ln p_i, \end{aligned} \quad (10)$$

where p_i is the probability of the site configuration i (temperature is expressed in energy units, whence entropy in natural units). In this paper we focus on liquid, i.e., homogeneous state, hence we assume that all sites have the same configuration probability distribution. The latter can then be obtained as a marginal of the tetrahedron distribution p_{ijkl} , by the following symmetrized expression

$$p_i = \sum_{j=0}^3 w_j \sum_{k=0}^3 w_k \sum_{l=0}^3 w_l \frac{p_{ijkl} + p_{ijk} + p_{klij} + p_{jkli}}{4}. \quad (11)$$

The free energy turns out to be a function of the only tetrahedron probability distribution, taken as variational parameter. The minimization with respect to such parameter, with the normalization constraint

$$\sum_{i=0}^3 w_i \sum_{j=0}^3 w_j \sum_{k=0}^3 w_k \sum_{l=0}^3 w_l p_{ijkl} = 1, \quad (12)$$

can be performed by the Lagrange multiplier method, yielding the equations

$$p_{ijkl} = \xi^{-1} e^{-\tilde{\mathcal{H}}_{ijkl}/T} (p_i p_j p_k p_l)^{3/4}, \quad (13)$$

where ξ , related to the Lagrange multiplier, can be computed by imposing the constraint Eq. (12) as

$$\xi = \sum_{i=0}^3 w_i \sum_{j=0}^3 w_j \sum_{k=0}^3 w_k \sum_{l=0}^3 w_l e^{-\tilde{\mathcal{H}}_{ijkl}/T} (p_i p_j p_k p_l)^{3/4}. \quad (14)$$

Eq. (13) is in a fixed point form, and can be solved numerically by simple iteration (natural iteration method³⁶). For the cluster-site approximation, the numerical procedure can be proved to reduce the free energy at each iteration^{34,36}, and therefore to converge to local minima. Let us notice that the symmetrized marginalization Eq. (11) imposes implicitly a homogeneity constraint, useful to investigate the metastable liquid properties. In fact it is easy to see that Eq. (13), due to invariance of $\tilde{\mathcal{H}}_{ijkl}$ under cycle permutation of the subscripts [see Eqs. (3) and (4)], determines a tetrahedron distribution p_{ijkl} with the same property, giving rise to four equal site marginals. Therefore, we must be aware that the stationary point we find may be unstable with respect to a translational symmetry breaking. Anyway, from the solution of Eq. (13) one obtains a tetrahedron probability distribution $\{p_{ijkl}\}$, whence one can compute the thermal average of every observable, the internal energy by Eq. (3) and the free energy by Eq. (10). The latter can be also related to the normalization constant as

$$\omega = -T \ln \xi, \quad (15)$$

whence ξ can be viewed as an effective (single site) grand canonical partition function. We shall make use of this property in the following.

IV. THERMODYNAMIC PROPERTIES

In order to investigate the model properties, let us fix a set of parameters. First of all, let us take $\epsilon/\eta = 0.25$. This value is equal to the one employed for a previous mean field analysis³⁷, and similar to the one chosen by RD for the original model²³. This choice accounts for the greater binding energy of hydrogen bonds with respect to Van der Waals interactions, and will be kept fixed throughout the present analysis. As far as the multiplicity of non-bonding water configurations is concerned, we set $w = 20$, to mimic the high directionality of hydrogen bonds. From the phase diagram analysis, it turns out that it is necessary to set this parameter large enough to let anomalous properties appear, but further increase does not change qualitatively the phase behavior. Therefore, also the latter parameter will be held fixed in the following. On the contrary, we shall investigate in detail the effect of changing the weakening parameter c , which is actually the crucial one for the present model, in the regime $c > 0.25$, according to Eq. (9).

A. Phase diagrams

Let us report in Fig. 4 a sequence of temperature-pressure (left column) and density-temperature (right column) phase diagrams, for different c values. Imposing homogeneity, our analysis includes both thermodynamically stable and metastable (supercooled) phases, even if stability is not investigated. Let us notice that pressure can be determined as $P = -\omega$, due to the fact that the free energy has been defined as a grand-canonical potential. We have assumed volume per site equal to 1, i.e., pressure is expressed in energy units.

For $c = 0.3$ we have essentially an ordinary liquid-vapor coexistence line, terminating at a critical point, even if an anomalous temperature dependence of the liquid density (without a maximum) can be observed. In the very low temperature region, an intermediate density liquid phase appear, giving rise to a triple point. This phase is actually an unphysical solution of our equations, in that the entropy turns out to be negative. In this region a crystalline phase is likely to be stable.

For $c = 0.4$ the phase diagram undergoes a dramatic change. The intermediate liquid phase region becomes a unique region with the ordinary liquid, and the triple point is replaced by a second critical point, where the low-high density liquid coexistence terminates. The second critical point still lies in a negative entropy region. The density of the liquid coexisting with the vapor displays a maximum as a function of temperature.

For $c = 0.5$ the density maximum becomes more pronounced, but there is no topological change in the phase diagram.

For $c = 0.6$ a new coexistence line appears between the high density and the low density liquid. Such a transition line (probably metastable) is negatively sloped in

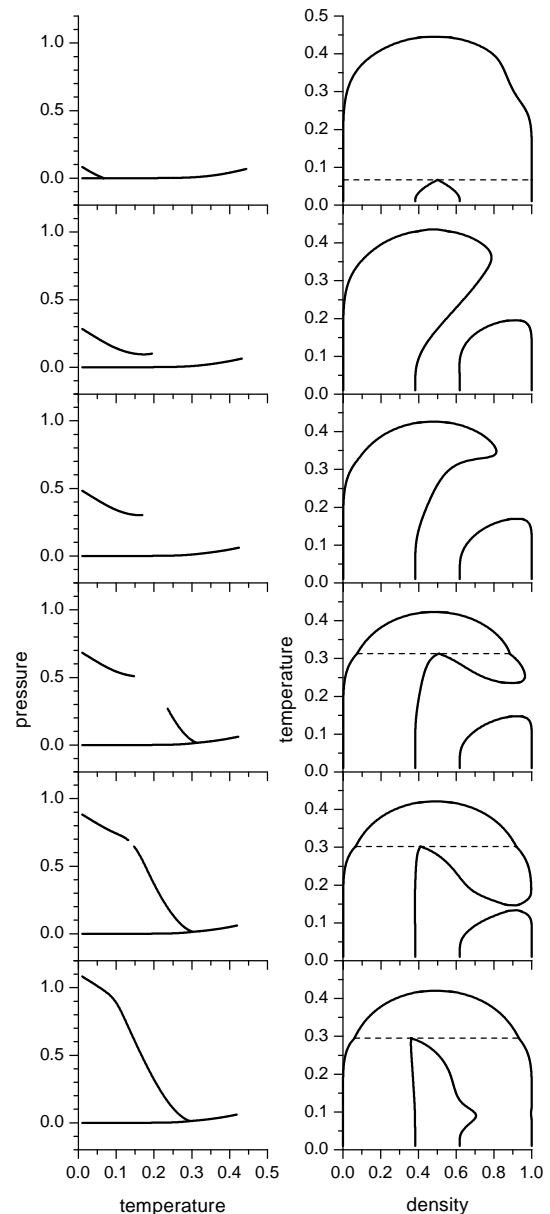


FIG. 4: Pressure (P/η) vs temperature (T/η) phase diagrams (left column) and temperature vs density (ρ) phase diagrams (right column) for $\epsilon/\eta = 0.25$ and $w = 20$. From top to bottom $c = 0.3, 0.4, 0.5, 0.6, 0.7, 0.8$, respectively. Thick solid lines denote (first order) phase transitions (left) and delimit coexistence regions (right). A thin dashed line (right) corresponds to three-phase coexistence (triple point).

the temperature-pressure phase diagram, and terminates at a third critical point. In this scenario, the ordinary liquid phase stability is delimited by a reentrant spinodal, as will be verified in the following. A similar scenario has been already observed in a two-dimensional model²⁸.

For $c = 0.7$ the two “metastable” critical points gets closer, and finally, for $c = 0.8$, they merge, giving rise to a unique high-low density liquid coexistence, which

terminates at a triple point. The topology of the phase diagram is again similar to the one obtained for low c values, but in this case there exists a region where the low density liquid has positive entropy. From a microscopical point of view, such a liquid phase is characterized by a high probability of bonding configurations, i.e., it is a highly hydrogen bonded phase. This feature corresponds to a lower density, as previously pointed out.

The role of the weakening parameter is well characterized by the sequence of temperature-pressure phase diagrams. Actually, the general trend is that, upon increasing c , the stability region of the low density liquid (having a low number of weakening molecules) gets larger and larger. In the next part of this work we focus on two particular parameter choices ($c = 0.4, 0.6$), as representatives of a range of c values in which the model results are qualitatively consistent with the anomalies observed for real liquid water in ordinary temperature and pressure conditions. The general analysis reported above is completed by studying the locus of density extrema (maxima and minima) as a function of temperature, the liquid phase spinodals, and the Kauzmann line, where the liquid entropy vanishes (ideal glass transition).

B. TED locus, spinodal, and Kauzmann line

One of the thermodynamic anomalies of the present model is the temperature of maximum density (TMD) along isobars for the liquid phase. Nevertheless, for some pressure range, it is possible to observe also a temperature of minimum density, therefore we shall generally speak about a temperature of extremum density (TED). Joining temperatures of maximum (or extremum) density at different pressures defines the so called TMD (or TED) locus. At ordinary pressure, the TMD locus is a negatively sloped line in the T - P phase diagram of real water. In principle, we could determine the TED locus numerically, by adjusting the chemical potential in order to fix the pressure and then imposing that the (isobaric) thermal expansion coefficient vanishes. Actually we have performed a different calculation, based on the effective partition function (15), rewritten as a function of only two variational parameters, namely, the density ρ and the fraction ϕ of bonding molecules. Details about this calculation, which allows to determine density response functions and spinodals as well, are given in the Appendix. The limit of stability of the liquid phase (spinodal) is the locus in which the metastable liquid ceases to be a minimum of the free energy, and becomes a saddle point. Actually, in the homogeneity hypothesis, we add a constraint to the free energy, thus neglecting stability loss with respect to symmetry broken (ice) phases. Aware of this, spinodals can be obtained by imposing that the hessian determinant of the homogeneous free energy (or partition function) vanishes, as shown in the Appendix. Let us notice that, in this case, it is not possible to work out the result making use of the natural

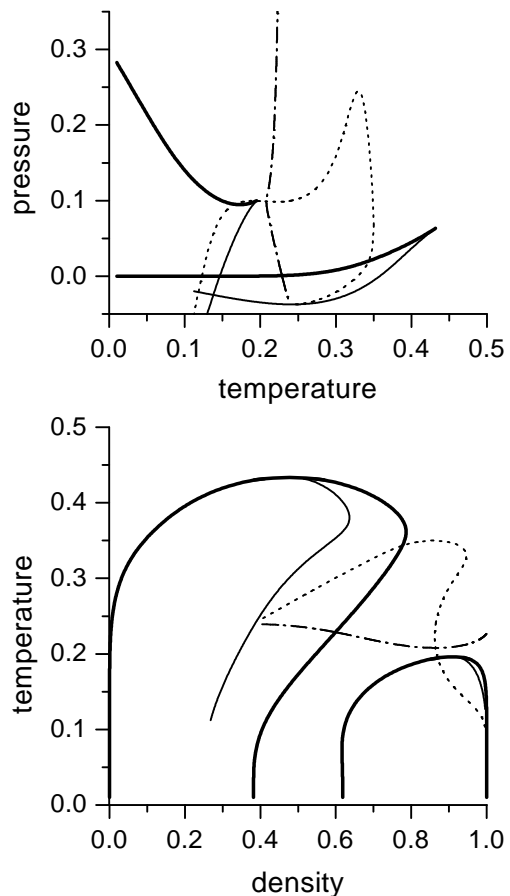


FIG. 5: Pressure (P/η) vs temperature (T/η) phase diagram (top panel) and temperature vs density (ρ) phase diagram (bottom panel) for $\epsilon/\eta = 0.25$, $w = 20$, $c = 0.4$. Thick solid lines denote (first order) phase transitions (top) and delimit coexistence regions (bottom). Thin (solid, dotted, and dash-dotted) lines denote spinodals, TED locus, and Kauzmann line, respectively.

iteration Eqs. (13), because the attraction basin of the liquid phase gets smaller and smaller, and vanishes at the spinodal. On the contrary, the locus at which the liquid phase entropy vanishes (Kauzmann line), can be easily determined numerically.

The results are shown in Figs. 5 and 6 for $c = 0.4$ and $c = 0.6$, respectively. In both cases, we find a density maximum as a function of temperature for liquid coexisting with vapor (and at constant pressure as well), and the TMD slightly decreases upon increasing pressure. Another common feature is the presence of a high-low density liquid coexistence, and of a corresponding critical point. For $c = 0.4$ the critical point lies in the negative entropy region, beneath the Kauzmann line, while for $c = 0.6$ it lies in the positive entropy region. The Kauzmann line displays a cusp (towards low temperature) in the vicinity of the critical point. The low approximation level of our analysis does not allow to take all of this

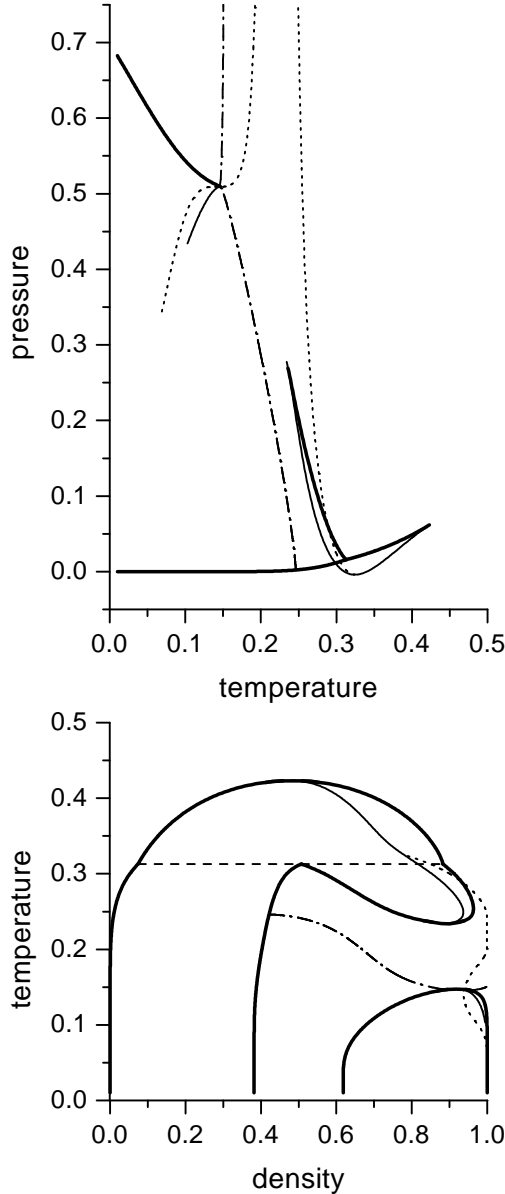


FIG. 6: Pressure (P/η) vs temperature (T/η) phase diagram (top panel) and temperature vs density (ρ) phase diagram (bottom panel) for $\epsilon/\eta = 0.25$, $w = 20$, $c = 0.6$. Thick solid lines denote (first order) phase transitions (top) and delimit coexistence regions (bottom). A thin dashed line (bottom) corresponds to three-phase coexistence (triple point). Thin (solid, dotted, and dash-dotted) lines denote spinodals, TED locus, and Kauzmann line, respectively.

information as reliable, but let us notice that a similar scenario has been predicted also by a statistical analysis of the potential energy landscape of simulated water, performed by Sciortino and coworkers on the basis of the inherent structure theory and of some simplifying assumptions³⁸. As far as the TMD locus is concerned, we observe a peculiar maximum in the T - P plane. For

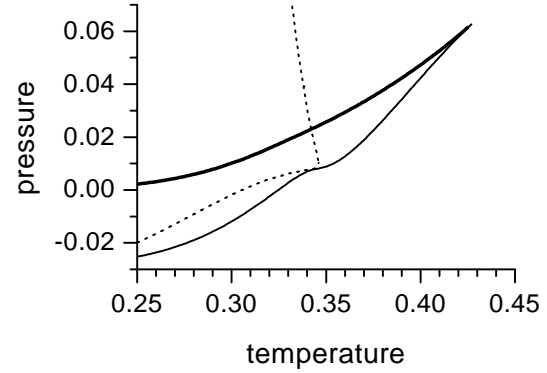


FIG. 7: Pressure (P/η) vs temperature (T/η) phase diagram for $\epsilon/\eta = 0.25$, $w = 20$, $c = 0.5$. A thick solid lines denotes the liquid-vapor transition. The thin (solid and dotted) lines denote the liquid spinodal and the TMD locus, respectively.

$c = 0.6$ the maximum occurs at a far higher pressure than for $c = 0.4$. After the maximum, upon decreasing temperature, the TMD locus becomes a temperature of minimum density locus, ending in the second critical point. After that, the line continues (again as a TMD locus) in the metastability region of the high density liquid with respect to the low density liquid. Upon decreasing pressure, we find the most relevant differences between the two cases. For $c = 0.4$, the TMD reaches a maximum and then decreases again, as we move in the negative pressure region. For $c = 0.6$, the TMD always increases. In both cases the TMD locus terminates against the liquid-vapor spinodal. In the T - P diagram, the meeting point corresponds to a minimum of the spinodal line, as required by the thermodynamic consistency arguments of Speedy and Debenedetti^{39,40,41,42,43}. Such a minimum is placed at a much higher temperature for $c = 0.6$ than for $c = 0.4$. As far as the liquid-vapor spinodal is concerned, another important difference is observed, namely, for $c = 0.6$ the spinodal reenters the positive pressure region, ending in the above mentioned “third” critical point. Such a reentrance gives rise to a divergence in the response functions, measured at constant pressure, as we shall see below. This is not the case for $c = 0.4$. As one could expect, it is possible to verify that the spinodal reenters the positive pressure region, if and only if the third critical point exists. The boundary between the two regimes is found to be around (actually a little greater than) $c = 0.5$. A region of the T - P phase diagram for $c = 0.5$, showing the reentrance of the TMD locus, is reported in Fig. 7.

C. Response functions

Let us now investigate the density response functions and the specific heat of the liquid at constant pressure $P/\eta = 0.05$, roughly corresponding to 1/10 of the liquid-vapor critical pressure. Also for this calculations, de-

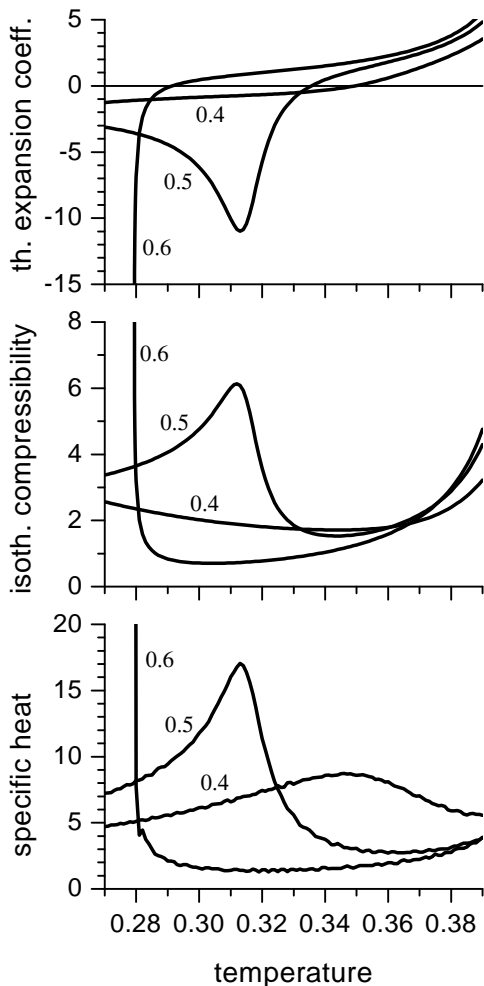


FIG. 8: Response functions at constant pressure ($P/\eta = 0.05$) for the liquid phase as a function of temperature (T/η), for $\epsilon/\eta = 0.25$ and $w = 20$. From top to bottom we show the isobaric thermal expansion coefficient ($\eta\alpha_P$), the isothermal compressibility ($\eta\kappa_T$), and the specific heat (c_P). Numerals beside each plot denote c values.

tails are left to the Appendix. We find anomalous behavior, similar to that of real liquid water. The first response function we consider is the thermal expansion coefficient $\alpha_P = (-\partial \ln \rho / \partial T)_P$, which, from statistical mechanics, is known to be proportional to the entropy-volume cross-correlation. For ordinary fluids, α_P is always positive, i.e., the local entropy and the local specific volume are positively correlated. On the contrary, for our model α_P (Fig. 8, top panel) is anomalous. As temperature is lowered, the expansion coefficient vanishes (at the TMD), and then becomes negative. For $c = 0.4$, we have observed just a shallow minimum (not shown) around $T/\eta = 0.17$. The minimum is more pronounced for $c = 0.5$, which, as mentioned above, is still in a regime where the third critical point does not exist. Finally, for $c = 0.6$, the minimum becomes a di-

vergence, due to the spinodal reentrance in the positive pressure region. Of course, the divergent behavior can be observed only for pressure values less than the third critical point pressure. The trend of the isothermal compressibility $\kappa_T = (\partial \ln \rho / \partial P)_T$ is also anomalous (Fig. 8, middle panel). For a typical liquid, κ_T decreases as one lowers temperature, because it is proportional to density fluctuations, whose magnitude decreases, upon decreasing temperature. On the contrary, we can observe that κ_T , once reached a minimum, begins to increase upon decreasing temperature. Only a broad maximum is observed for $c = 0.4$; the maximum becomes sharper for $c = 0.5$, and finally becomes a divergence for $c = 0.6$. The constant pressure specific heat $c_P = (-T\partial^2 \mu / \partial T^2)_P$ (Fig. 8, bottom panel) displays a completely analogous behavior, with the minimum occurring at a higher temperature. Qualitatively similar thermodynamic anomalies are observed in real liquid water, even if the possibility of divergent-like behavior in the supercooled regime is no longer believed to be realistic³.

D. A comparison with the RD model

Let us finally report the results of a comparison with the RD model, of which, as previously mentioned, the present model is a simplified version. In particular, let us consider the results of a Monte Carlo simulation²⁹, in which parameters were chosen to push the low-high density liquid critical point to a temperature of the same order of magnitude of the ordinary liquid-vapor critical point. In this work, evidence was given that the model actually predicts liquid-liquid coexistence, and that the latter is not an artifact of approximations. The model parameters are $\epsilon/\eta = 0.2$, $c = 0.8$, while the total number of molecule orientations is $q = 108$. In order to a comparison, the latter parameter is to be renormalized, in that RD model molecules, possessing bonding arms of two different kinds (donors and acceptors), allow 12 different bonding configurations, while the present model allows only 2. We have performed the renormalization as follows

$$\frac{q}{12} = \frac{w+2}{2}, \quad (16)$$

obtaining $w = 16$. The results are reported in Fig. 9. The topology of the (temperature-density) phase diagram is qualitatively similar, and also the quantitative agreement of critical temperatures is good. Only the density of the liquid coexisting with the vapor displays a significant discrepancy. The reentrance in the liquid-liquid coexistence region at low temperature is reproduced, even if RD conjecture that a lower critical point exists, mainly on the basis of first order approximation results²³, whereas we find coexistence down to zero temperature. Anyway, as shown before, the presence or absence of a lower critical point may be induced by small c value variations.

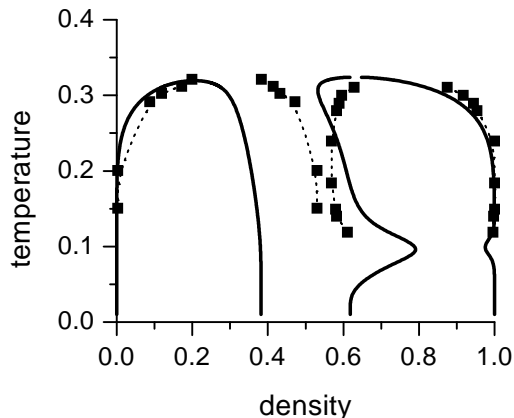


FIG. 9: Temperature (T/η) vs. density (ρ) phase diagram for $\epsilon/\eta = 0.2$, $w = 16$, $c = 0.8$ (solid lines), compared to Monte Carlo results from Ref. 29 (scatters). Dotted lines are eyeguides.

V. DISCUSSION AND CONCLUSIONS

In this paper we have investigated a lattice fluid model with water-like features, by a generalized first order approximation. As mentioned in the Introduction, the mechanism by which our model describes water anomalies is essentially based on the competition between the Van der Waals isotropic interaction and the highly directional H bonding interaction, and on the difference between the respective optimal interaction distances. In the lattice framework, the latter is taken into account by means of the weakening trick, proposed by RD²³. We have actually simplified the original RD model by neglecting the distinction between H bond donors and acceptors. In spite of this, the model turns to reproduce qualitatively several thermodynamic anomalies of real water at constant pressure: a maximum of density, and a minimum of isothermal compressibility and specific heat. This fact confirms the idea that the distinction between donors and acceptors is not crucial to the physics of H bonding²⁴. By a suitable parameter scaling, we have also compared some results of the simplified model with those of the original model obtained by Monte Carlo simulations, and we have verified that the simplification and the approximation seem to preserve the qualitative features of the phase diagram, though in a case of quite simple topology. On the simplified model, it is possible to perform a generalized first order approximation on a tetrahedron cluster, without introducing further “ad hoc” approximations, as it was necessary in the original paper by RD²³. Moreover, with respect to Monte Carlo simulations, the first order approximation has not only the advantage of a much lower computational effort, but also allows a well defined extrapolation of the equation of state in the supercooled regime, without the need of criteria to prevent the simulation dynamics from falling into crystalline states. In fact, analysis of the model predic-

tions in the metastable phase region is extremely interesting to rationalize observed thermodynamic anomalies.

As previously shown, there is evidence of a second (metastable) critical point, which terminates a line of first order transitions between two liquid phases at different densities. For $c \lesssim 0.5$, the second critical point lies at a temperature lower than the Kauzmann temperature, at which the configurational entropy vanishes. Moreover, the Kauzmann line displays a reentrance in the vicinity of the second critical point. All of these features turn out to be in a remarkably good agreement with the simplified statistical analysis of the potential energy landscape of simulated water, recently performed by Sciortino and coworkers³⁸.

We have also computed the temperature of extremum density locus and the liquid spinodals, in the framework of our approximation. In the ordinary temperature and pressure region, the TED locus is a negatively sloped line (in the T - P diagram) corresponding to a density maximum, as observed in experiments. The locus displays a pressure maximum, and, for higher pressure values, the liquid becomes normal. After the maximum, upon decreasing temperature, the TED line denotes a minimum density, which is a peculiar feature of our model. The TED line crosses the Kauzmann line very close to its reentrance, as recently predicted by Speedy⁴⁴. On the other side, the TED line is reentrant for low c values and it is not for higher c values. In both cases it terminates at a minimum of the spinodal in the T - P plane, as required by thermodynamic consistency³⁹. Nevertheless, in the former case the spinodal does not reenter the positive pressure half-plane, while in the latter case it does. In this case, response functions exhibit a divergent behavior. Such results are interesting in that the reentrant spinodal was one of the conjectures invoked to explain thermodynamic anomalies of water^{39,45}. The fact, that the same model with different parameter values may predict or not a reentrant spinodal, suggests that in real water there is probably a subtle balance of interactions, which does not allow to discriminate easily between the two possible scenarios. This fact has been previously pointed out by phenomenological models⁵, but, to our knowledge, not yet by microscopical models. The most recent and accurate molecular dynamics simulations suggest a scenario with a non-reentrant spinodal and a reentrant (“nose shaped”) TMD locus³. The present model accounts for such a scenario for $c \approx 0.5$. In this case, a slight reentrance of the spinodal, induced by the vicinity of the TMD locus, can be observed. A similar “intermediate” situation is consistent with the results of an analytical equation of state derived by Truskett et al.⁴⁶. We have remarked this feature in that it may justify the early experimental results which supported the reentrant spinodal conjecture⁴⁵.

As a conclusion, let us remind that the model in the present treatment is not able to provide microscopic structural details as simulations do, but its most appealing feature is simplicity. In spite of how little we put in the model, the latter turns out to give a qualitatively cor-

rect description of the peculiar thermodynamics of water, and is consistent with predictions based on much more sophisticated models and simulations. Therefore, we suggest that it may be suitable as a starting point to investigate complex phenomena, such as the solvation of apolar solutes, in which the physics of hydrogen bonding plays a significant role.

APPENDIX: SPINODALS AND RESPONSE FUNCTIONS

In this appendix we report in detail the calculation of the spinodal lines and of the density response functions, i.e., the (isobaric) thermal expansion coefficient α_P and the isothermal compressibility κ_T . The (isobaric) heat capacity c_P is determined by a numerical derivative of the chemical potential μ , which comes out in a natural way from the same calculation, as a function of temperature and pressure.

Eq. (15) suggests that the normalization constant ξ [Eq. (14)] can be used as a variational form of the effective (single site) grand canonical partition function, to be maximized with respect to the site probability distribution p_i . We can also observe that the homogeneous liquid phase is isotropic, whence the 2 bonding configurations on each site must have the same probability

$$p_1 = p_2. \quad (\text{A.1})$$

With the above assumption, we can replace the fourfold summation over the configurations i, j, k, l of a tetrahedron with a double summation over the number $n = 0, \dots, 4$ of occupied sites and the number $k = 0, \dots, n$ of molecules in a bonding configuration. There are $\binom{4}{n}\binom{n}{k}$ ways of arranging molecules with the above requirements, and the multiplicity of the resulting configuration (k bonding molecules and $n - k$ non bonding ones) is $2^k w^{n-k}$, whence we obtain

$$\xi = \sum_{n=0}^4 \sum_{k=0}^n \binom{4}{n} \binom{n}{k} 2^k w^{n-k} (p_0^{4-n} p_1^k p_3^{n-k})^{3/4} x_{n,k}, \quad (\text{A.2})$$

where $x_{n,k}$ are linear combinations of the Boltzmann weights $e^{-\tilde{\mathcal{H}}_{ijkl}/T}$, appearing in Eq. (13). They are obtained as described in Tab. I. In order to avoid imposing the normalization constraint, it is convenient to rewrite the site probabilities as a function of the density ρ (occupation probability) and the fraction ϕ of molecules in a bonding configuration. It is easy to obtain

$$p_0 = 1 - \rho \quad (\text{A.3})$$

$$p_1 = \frac{\rho\phi}{2} \quad (\text{A.4})$$

$$p_3 = \frac{\rho(1-\phi)}{w}, \quad (\text{A.5})$$

n	k	$\binom{4}{n}$	$\binom{n}{k}$	$x_{n,k}/z^{n/4}$
0	0	1	1	1
1	0	4	1	1
1	1	4	1	1
2	0	6	1	$\frac{1}{3} + \frac{2}{3}e^{\epsilon/T}$
2	1	6	2	$\frac{1}{3} + \frac{2}{3}e^{\epsilon/T}$
2	2	6	1	$\frac{1}{3} + \frac{2}{3}e^{\epsilon/T} \left(\frac{3}{4} + \frac{1}{4}e^{\eta/T} \right)$
3	0	4	1	$e^{2\epsilon/T}$
3	1	4	3	$e^{2\epsilon/T}$
3	2	4	3	$e^{2\epsilon/T} \left\{ \frac{1}{3} + \frac{2}{3} \left[\frac{3}{4} + \frac{1}{4}e^{\eta(1-c/2)/T} \right] \right\}$
3	3	4	1	$e^{2\epsilon/T} \left[\frac{1}{2} + \frac{1}{2}e^{\eta(1-c/2)/T} \right]$
4	0	1	1	$e^{4\epsilon/T}$
4	1	1	4	$e^{4\epsilon/T}$
4	2	1	6	$e^{4\epsilon/T} \left\{ \frac{1}{3} + \frac{2}{3} \left[\frac{3}{4} + \frac{1}{4}e^{\eta(1-c)/T} \right] \right\}$
4	3	1	4	$e^{4\epsilon/T} \left[\frac{1}{2} + \frac{1}{2}e^{\eta(1-c)/T} \right]$
4	4	1	1	$e^{4\epsilon/T} \left[\frac{1}{8} + \frac{6}{8}e^{\eta(1-c)/T} + \frac{1}{8}e^{2\eta(1-c)/T} \right]$

TABLE I: $x_{n,k}$ coefficients. The way they have been computed is explained hereafter. The chemical potential is taken into account by the $z^{n/4}$ prefactor, where $z \equiv e^{\mu/T}$ is the fugacity. For $n = 0, 1$ no interaction is possible, whence only the fugacity term is present. For $n = 2$ there are 6 possible arrangements of molecules on the sites; in 2 of them (1/3) the 2 molecules are not NNs and there is no interaction; in the remaining 4 cases (2/3) the 2 molecules are NNs and interact with the Van der Waals energy (whence the factor $e^{\epsilon/T}$). Only when $k = 2$ a H bond can occur (whence the factor $e^{\eta/T}$), in 1 out of 4 possible configurations of 2 bonding molecules, i.e., when the molecules point an arm to each other. The H bond is not weakened because the neighbor sites are empty. For $n = 3$ all possible arrangements have 2 pairs of NN molecules, whence the factor $e^{2\epsilon/T}$. If $k = 0, 1$ no other interaction exists. If $k = 2$ we can place the 2 bonding molecules on NN sites in 2/3 of the cases, and in 1/4 of their allowed configuration they form a H bond, which is half weakened, because one of the NN sites is occupied. With $k = 3$ bonding molecules, there are $2^3 = 8$ possible configurations, 4 of which have 1 formed bond. For $n = 4$ all sites are occupied and there are 4 NN pairs, whence the factor $e^{4\epsilon/T}$. With $k = 0, 1$ bonding molecules, no other interaction is possible. With $k = 2$, there are $4/6 = 2/3$ arrangements in which the bonding molecules are placed on NN sites and form a H bond in 1/4 of their configurations. The bond is fully weakened, because both the neighbor sites are occupied. With $k = 3$ bonding molecules, the explanation is equivalent to the $n = 3$ case. Finally, with $k = 4$ bonding molecules, it is necessary to enumerate all the $2^4 = 16$ configurations, 2 of which have no bond, 6 have 1 bond, and 2 have 2 bonds.

whence

$$\xi = \sum_{n=0}^4 \binom{4}{n} f_{4,n}^{3/4}(\rho) \sum_{k=0}^n \binom{n}{k} (2^k w^{n-k})^{1/4} f_{n,k}^{3/4}(\phi) x_{n,k}, \quad (\text{A.6})$$

where

$$f_{n,k}(x) \equiv x^k(1-x)^{n-k}. \quad (\text{A.7})$$

In order to impose thermodynamic equilibrium, we have to minimize ξ with respect to the variational parameters ρ and ϕ . Let us notice that ξ also depends on the temperature T and the chemical potential μ (or equivalently the fugacity $z = e^{\mu/T}$), as appropriate in the grand-canonical ensemble. Such a dependence is hidden in the $x_{n,k}$ coefficients (see Tab. I). We impose the necessary minimum condition, by setting the derivatives of ξ with respect to ρ and ϕ to zero. Moreover, we are interested in working at fixed pressure P , therefore we have to impose a third equation $\omega = -P$, where, from Eq. (15), we have $\omega = -T \log \xi$. We have thus to solve a system of three equations

$$\frac{\partial \xi}{\partial(\ln \rho)} = 0 \quad (\text{A.8})$$

$$\frac{\partial \xi}{\partial(\ln \phi)} = 0 \quad (\text{A.9})$$

$$\xi - e^{P/T} = 0, \quad (\text{A.10})$$

which is actually an implicit definition of the three functions $\rho(T, P)$, $\phi(T, P)$, and $z(T, P)$. Having determined numerically the fugacity $z(T, P)$, we immediately obtain the chemical potential $\mu = T \log z$, whence the specific heat $c_P = (-T \partial^2 \mu / \partial T^2)_P$ by a numerical derivative.

Let us now consider the three simultaneous Eqs. (A.8), (A.9), and (A.10). As previously mentioned, the left hand sides are functions of ρ, ϕ, z, T, P . If we replace ρ, ϕ, z by the previously determined functions of T, P , we obtain three functions that are identically equal to 0, for each value of T and P . Therefore, taking the partial derivatives with respect to $X = T, P$, we obtain the following linear system:

$$\mathbf{A} \cdot \begin{pmatrix} \frac{\partial(\ln \rho)}{\partial X} \\ \frac{\partial(\ln \phi)}{\partial X} \\ \frac{\partial(\ln z)}{\partial X} \end{pmatrix} = - \begin{pmatrix} \frac{\partial^2 \xi}{\partial(\ln \rho) \partial X} \\ \frac{\partial^2 \xi}{\partial(\ln \phi) \partial X} \\ \frac{\partial \xi}{\partial X} - e^{P/T} \frac{\partial(P/T)}{\partial X} \end{pmatrix}, \quad (\text{A.11})$$

where

$$\mathbf{A} = \begin{pmatrix} \frac{\partial^2 \xi}{\partial(\ln \rho)^2} & \frac{\partial^2 \xi}{\partial(\ln \rho) \partial(\ln \phi)} & \frac{\partial^2 \xi}{\partial(\ln \rho) \partial(\ln z)} \\ \frac{\partial^2 \xi}{\partial(\ln \phi) \partial(\ln \rho)} & \frac{\partial^2 \xi}{\partial(\ln \phi)^2} & \frac{\partial^2 \xi}{\partial(\ln \phi) \partial(\ln z)} \\ \frac{\partial \xi}{\partial(\ln \rho)} & \frac{\partial \xi}{\partial(\ln \phi)} & \frac{\partial \xi}{\partial(\ln z)} \end{pmatrix} \quad (\text{A.12})$$

and

$$\frac{\partial(P/T)}{\partial T} = -\frac{P}{T^2} \quad (\text{A.13})$$

$$\frac{\partial(P/T)}{\partial P} = \frac{1}{T}. \quad (\text{A.14})$$

The derivatives of ξ can be easily determined from Eq. (A.6), making use of

$$\frac{df_{n,k}^a(x)}{d(\ln x)} = \frac{a(k-nx)}{1-x} f_{n,k}^a(x) \quad (\text{A.15})$$

$$\frac{d^2 f_{n,k}^a(x)}{d(\ln x)^2} = \frac{a^2(k-nx)^2 - a(n-k)x}{(1-x)^2} f_{n,k}^a(x), \quad (\text{A.16})$$

obtained from Eq. (A.7), a being a generic exponent, and of

$$\frac{\partial x_{n,k}}{\partial(\ln z)} = \frac{n}{4} x_{n,k}, \quad (\text{A.17})$$

while $\partial x_{n,k} / \partial T$ can be obtained from Table I. In order to determine the density response function, we solve Eq. (A.11) with respect to $\partial(\ln \rho) / \partial X$, making use of the Kramer's rule, yielding

$$\frac{\partial(\ln \rho)}{\partial X} = \frac{\det \mathbf{B}}{\det \mathbf{A}}, \quad (\text{A.18})$$

where \mathbf{B} is obtained by replacing the right hand side of Eq. (A.11) in the first column of \mathbf{A} . In this way the isobaric thermal expansion coefficient $\alpha_P = -\partial(\ln \rho) / \partial T$ and the isothermal compressibility $\kappa_T = \partial(\ln \rho) / \partial P$ are expressed as a function of ρ, ϕ, z, T, P . As previously mentioned, ρ, ϕ, z can be determined numerically as a function of T, P , for instance by solving the simultaneous Eqs. (A.8), (A.9), and (A.10). As far as the TED locus is concerned, we have to add a fourth equation, imposing $\alpha_P = 0$. Finally, spinodal lines can be obtained as the locus in which the above response functions diverge, that is, $\det \mathbf{A} = 0$. Let us observe that, in the latter case, only three simultaneous equations are needed. In fact, if the grand canonical equilibrium conditions (A.8) and (A.9) are verified, the first two elements of the third line of \mathbf{A} (which we may denote by A_{31}, A_{32}) vanish, therefore we can write $\det \mathbf{A} = A_{33} \det \mathbf{A}_{33}$, where \mathbf{A}_{33} is the submatrix of \mathbf{A} obtained by removing the third row and the third column. As a consequence, the equation $\det \mathbf{A} = 0$ does not contain P . Solving the latter simultaneously with Eqs. (A.8) and (A.9), which do not depend on P as well, allows to determine $\rho(T)$, $\phi(T)$, and $z(T)$ defining the spinodal line. Then one can determine $\xi(T)$ by means of Eq. (A.6), and finally $P(T) = T \ln \xi(T)$.

-
- ¹ D. Eisenberg and W. Kauzmann, *The Structure and Properties of Water* (Oxford University Press, Oxford, 1969).
 - ² F. Franks, ed., *Water: a Comprehensive Treatise* (Plenum Press, New York, 1982).
 - ³ H. E. Stanley et al., J. Stat. Phys. **110**, 1039 (2003).
 - ⁴ H. E. Stanley et al., Physica A **257**, 213 (1998).
 - ⁵ P. H. Poole, F. Sciortino, T. Grande, H. E. Stanley, and C. A. Angell, Phys. Rev. Lett. **73**, 1632 (1994).
 - ⁶ H. S. Frank and M. W. Evans, J. Chem. Phys. **13**, 507 (1945).
 - ⁷ F. H. Stillinger, Science **209**, 451 (1980).
 - ⁸ K. A. Dill, Biochemistry **29**, 7133 (1990).
 - ⁹ F. H. Stillinger and A. Rahman, J. Chem. Phys. **60**, 1545 (1974).
 - ¹⁰ W. L. Jorgensen et al., J. Chem. Phys. **79**, 926 (1983).
 - ¹¹ M. W. Mahoney and W. L. Jorgensen, J. Chem. Phys. **112**, 8910 (2000).
 - ¹² H. E. Stanley et al., Physica A **315**, 281 (2002).
 - ¹³ G. M. Bell and D. A. Lavis, J. Phys. A **3**, 568 (1970).
 - ¹⁴ A. Ben-Naim, J. Chem. Phys. **54**, 3682 (1971).
 - ¹⁵ G. M. Bell, J. Phys. C **5**, 889 (1972).
 - ¹⁶ D. A. Lavis, J. Phys. C **6**, 1530 (1973).
 - ¹⁷ G. M. Bell and D. W. Salt, J. Chem. Soc., Faraday Trans. II **72**, 76 (1976).
 - ¹⁸ D. A. Lavis and N. I. Christou, J. Phys. A **10**, 2153 (1977).
 - ¹⁹ D. A. Lavis and N. I. Christou, J. Phys. A **12**, 1869 (1979).
 - ²⁰ P. H. E. Meijer, R. Kikuchi, and E. V. Royen, Physica A **115**, 124 (1982).
 - ²¹ D. A. Huckaby and R. S. Hanna, J. Phys. A **20**, 5311 (1987).
 - ²² S. Sastry, F. Sciortino, and H. E. Stanley, J. Chem. Phys. **98**, 9863 (1993).
 - ²³ C. J. Roberts and P. G. Debenedetti, J. Chem. Phys. **105**, 658 (1996).
 - ²⁴ K. A. T. Silverstein, A. D. J. Haymet, and K. A. Dill, J. Am. Chem. Soc. **120**, 3166 (1998).
 - ²⁵ H. E. Stanley et al., Physica A **205**, 122 (1994).
 - ²⁶ A. Patrykiewicz, O. Pizio, and S. Sokolowski, Phys. Rev. Lett. **83**, 3442 (1999).
 - ²⁷ P. Bruscolini, A. Pelizzola, and L. Casetti, Phys. Rev. Lett. **88**, 089601 (2002).
 - ²⁸ C. Buzano, E. de Stefanis, A. Pelizzola, and M. Pretti, Phys. Rev. E **69**, (to be published) (2003).
 - ²⁹ C. J. Roberts, A. Z. Panagiotopoulos, and P. G. Debenedetti, Phys. Rev. Lett. **77**, 4386 (1996).
 - ³⁰ K. A. T. Silverstein, A. D. J. Haymet, and K. A. Dill, J. Chem. Phys. **111**, 8000 (1999).
 - ³¹ R. Kikuchi, Phys. Rev. **81**, 988 (1951).
 - ³² G. An, J. Stat. Phys. **52**, 727 (1988).
 - ³³ T. Morita, J. Math. Phys. **13**, 115 (1972).
 - ³⁴ M. Pretti, J. Stat. Phys. **11**, 993 (2003).
 - ³⁵ W. A. Oates, F. Zhang, S. L. Chen, and Y. A. Chang, Phys. Rev. B **59**, 11221 (1999).
 - ³⁶ R. Kikuchi, J. Chem. Phys. **60**, 1071 (1974).
 - ³⁷ C. Buzano and M. Pretti, J. Chem. Phys. **119**, 3791 (2003).
 - ³⁸ P. T. F. Sciortino, E. La Nave, Phys. Rev. Lett. **91**, 155701 (2003).
 - ³⁹ R. J. Speedy, J. Phys. Chem. **86**, 982 (1982).
 - ⁴⁰ R. J. Speedy, J. Phys. Chem. **86**, 3002 (1982).
 - ⁴¹ R. J. Speedy, J. Phys. Chem. **91**, 3354 (1987).
 - ⁴² P. Debenedetti and M. C. D'Antonio, J. Chem. Phys. **84**, 3339 (1986).
 - ⁴³ P. Debenedetti and M. C. D'Antonio, J. Chem. Phys. **86**, 2229 (1987).
 - ⁴⁴ A. R. Imre, H. J. Maris, and P. R. Williams, eds., *Liquids Under Negative Pressure* (Kluwer Academic Publisher, Boston, 2002).
 - ⁴⁵ Q. Zheng, D. J. Durben, G. H. Wolf, and C. A. Angell, Science **254**, 829 (1991).
 - ⁴⁶ T. M. Truskett, P. G. Debenedetti, S. Sastry, and S. Torquato, J. Chem. Phys. **111**, 2647 (1999).